Research on Performance Optimization of Liquid Concentration Detection Systems Based on Turbulence Elimination

Authors:

Zhiyang Li, Haizeng Liu, Chao Wang, Jianye Chen, Qingsong Zhang

Date Submitted: 2023-02-17

Keywords: concentration detection, differential pressure, turbulence elimination structure, numerical simulation, optimal operating conditions

Abstract:

Liquid concentration detection systems have been widely used in food, chemical, pharmaceutical, and many other industries. When the liquid flows, a large number of vortices will usually be generated, resulting in increased turbulence intensity, which will interfere with the detection of the concentration of the suspension. In this paper, a method for concentration detection by differential pressure based on turbulence elimination is proposed to improve the reliability of concentration detection results. The changes in the internal flow field corresponding to different lengths of the turbulence elimination structure and different inlet angles are analyzed through numerical simulation. Finally, the influence of changes in structure parameters on the accuracy of concentration detection is tested through experiments. The results show that when the length of the turbulence elimination structure is small, the vortex zone inside the concentration detection device changes with the inlet velocity. When the length of the turbulence elimination structure is 150 mm, the vortex zone is basically not affected by the inlet velocity. The stability of the flow field increases with the increase in the inlet angle. When the inlet angle increases to 60°, a stable zone of turbulence will form in the region where Y > 0.4 m. When the length of the turbulence elimination structure is 150 mm and the inlet angle is 60°, the expected experimental results are obtained, and the actual needs of liquid concentration measurement are met.

Record Type: Published Article

Submitted To: LAPSE (Living Archive for Process Systems Engineering)

Citation (overall record, always the latest version):	LAPSE:2023.0120
Citation (this specific file, latest version):	LAPSE:2023.0120-1
Citation (this specific file, this version):	LAPSE:2023.0120-1v1

DOI of Published Version: https://doi.org/10.3390/pr11010085

processes

MDPI

Article

Research on Performance Optimization of Liquid Concentration Detection Systems Based on Turbulence Elimination

Zhiyang Li, Haizeng Liu *, Chao Wang, Jianye Chen and Qingsong Zhang

School of Materials Science and Engineering, Anhui University of Science and Technology, Huainan 232001, China
* Correspondence: liuhzeng@163.com; Tel.: +86-135-0554-0645

Abstract: Liquid concentration detection systems have been widely used in food, chemical, pharmaceutical, and many other industries. When the liquid flows, a large number of vortices will usually be generated, resulting in increased turbulence intensity, which will interfere with the detection of the concentration of the suspension. In this paper, a method for concentration detection by differential pressure based on turbulence elimination is proposed to improve the reliability of concentration detection results. The changes in the internal flow field corresponding to different lengths of the turbulence elimination structure and different inlet angles are analyzed through numerical simulation. Finally, the influence of changes in structure parameters on the accuracy of concentration detection is tested through experiments. The results show that when the length of the turbulence elimination structure is small, the vortex zone inside the concentration detection device changes with the inlet velocity. When the length of the turbulence elimination structure is 150 mm, the vortex zone is basically not affected by the inlet velocity. The stability of the flow field increases with the increase in the inlet angle. When the inlet angle increases to 60°, a stable zone of turbulence will form in the region where Y > 0.4 m. When the length of the turbulence elimination structure is 150 mm and the inlet angle is 60°, the expected experimental results are obtained, and the actual needs of liquid concentration measurement are met.

Keywords: concentration detection; differential pressure; turbulence elimination structure; numerical simulation; optimal operating conditions

Citation: Li, Z.; Liu, H.; Wang, C.; Chen, J.; Zhang, Q. Research on Performance Optimization of Liquid Concentration Detection Systems Based on Turbulence Elimination. *Processes* **2023**, *11*, 85. https://doi.org/10.3390/pr11010085

Academic Editor: Li Xi

Received: 3 December 2022
Revised: 16 December 2022
Accepted: 21 December 2022
Published: 28 December 2022

1. Introduction

Accurate detection of the liquid concentrations is very important for many industries and production processes, including food processing, the chemical industry, and the pharmaceutical industry [1–3]. Researchers around the world have studied some related parameters, such as solid content, particle distribution, and flow rate [4–6]. At present, the most commonly used detection techniques include optical methods, acoustic methods, and differential pressure methods [7,8].

The effect of light scattering is produced when light rays are projected onto waterborne particles. Optical detection methods use such effects to perform detection tasks [9]. Such methods are mostly used to measure the content of particles suspended in the water and the turbidities of liquids, and have been widely used in water quality monitoring and water treatment [10,11]. Early optical detection methods, such as the Jackson Candle Turbidimeter, mainly rely on the human eye to identify different turbidities. These methods cannot perform automatic detection, and their detection accuracy is relatively low. For these reasons, such methods cannot be used for detection in turbulent flows [11,12]. The precision of commonly used turbidity meters has been improved, and these turbidity meters are used more often for turbidity detection in low-turbidity liquids and for the processing of small samples [12,13]. Acoustic detection methods obtain detection results relying on the reflection of acoustic waves. Such methods are usually used to measure the concentrations of suspensions [14,15]. However, the computational model of an acoustic detection method

usually involves an ideal flow field, and the detection accuracy is greatly affected by the flow field [16]. In some complex spaces, the accuracy of acoustic detection methods may decrease [17]. For instance, when a suspension contains unusual substances, the attenuation of acoustic waves may increase, and the acoustic waves may not be transmitted to the receiver [18]. For liquids with complex flow fields, such as dynamic liquids that flow in pipelines or liquids that can generate noise or bubbles when flowing [19–21], the detection results produced by acoustic detection methods are not ideal.

Differential pressure methods are indirect detection methods that detect the concentrations of suspensions by calculating the pressure difference between the suspensions at different heights. The detection results of such methods are less affected by the flow field and the properties of the liquid to be measured. Moreover, such methods have several merits, such as low cost and clear physical interpretation. Due to these merits, such methods have been widely used [22,23]. In this paper, a technique for concentration detection by differential pressure based on turbulence elimination is proposed. In this method, a turbulence elimination structure is used to create a stable flow field, thus enabling accurate concentration detection [24]. The turbulent flow in the internal flow field of the concentration detection device under different structure parameters is simulated using the fluent software to identify its characteristics, and the influence of the characteristics of turbulent flow on the detection results and the regulation mechanism are analyzed.

2. Concentration Detection Device and Principle

Experimental Device

Figure 1 shows the differential pressure concentration measurement device and concentration measurement experimental system. The experimental system mainly includes the following components: circulating water tank, water pump, valve, flowmeter, inlet nozzle, turbulence elimination structure, observation tank, sensor and overflow tank.

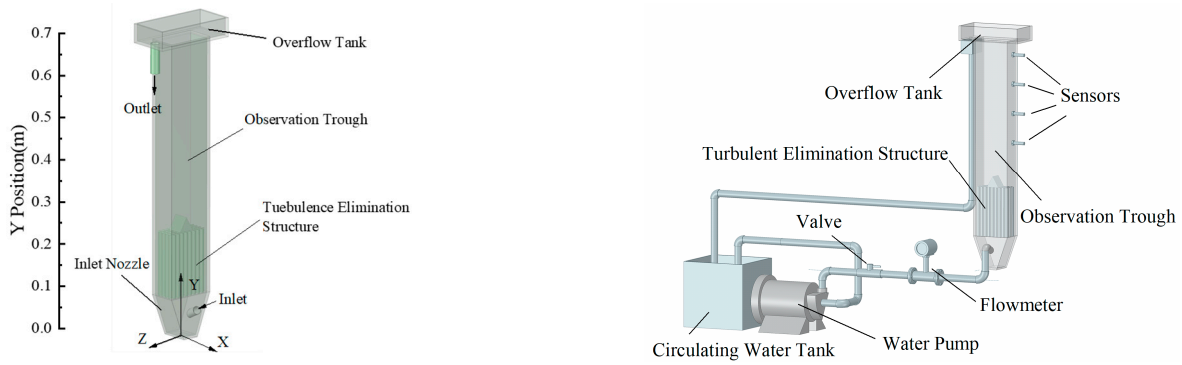

Figure 1. Differential pressure-based concentration detection device and system. (**a**) Differential pressure-based concentration detection device. (**b**) Differential pressure-based concentration detection system.

In a homogeneous solution or suspension, two pressures will be generated at different heights. In a vertical pipeline, the flow velocity of liquid remains constant at different positions, i.e., $u_1 = u_2$. As shown in Figure 2, according to the relevant knowledge of fluid mechanics, the following formula can be obtained:

$$\Delta P = \rho g \Delta H \tag{1}$$

where ΔP is the pressure difference detected by sensors at different positions, ΔH is the difference between the vertical heights of different sensors, and ρ is the density of the liquid.

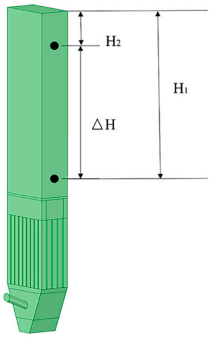

Figure 2. Schematic diagram of the concentration detection principle.

For a suspension, the relationship between concentration and density can be expressed as:

$$C_w = \frac{(\rho - 1)\rho_m}{\rho_m - 1} \times 1000 \quad (2)$$

where C_w is the concentration of the suspension, and ρ_m is the density of solids in the suspension.

When the liquid to be detected flows through the pipeline, it has complex flow regimes and generates a large number of air bubbles. A TES is incorporated into the system to reduce the turbulence intensity of the flow and remove air bubbles from the flow. After the state of the flow in the upper section of the concentration detection device has stabilized, the stability and accuracy of pressure sensor readings will be greatly improved, which is favorable for the further optimization of the device and the determination of the device's optimal operating conditions.

Structure parameters have great influence on the internal flow field of the detection device, and the internal flow field will affect the readings of pressure sensors. The purpose of the experiments is to investigate the effect of flow field changes caused by different structure parameters on the differential pressure. During the experiments, the inlet velocity (V) was set to 0.3 m/s, 0.4 m/s, 0.5 m/s, 0.6 m/s, 0.7 m/s, 0.8 m/s and 0.9 m/s, respectively, and five separate experiments were designed for each inlet velocity. Pressure sensors were installed at fixed positions, and the difference between their heights was measured: ΔH = 20 cm. During each separate experiment, after the flow field stabilized, the readings of all sensors were taken within five seconds. The average value of these readings was taken as the final result of the experiment, which was used to verify the effectiveness and validity of measurement under the current experimental conditions.

3. Numerical Simulation

3.1. Computing Domains and Grids

A three-dimensional (3D) model of the concentration detection device was built. The internal flow field was divided into grids in the grid module, and the gridding results were uploaded into the fluent software. To improve the quality of model grids, structured grids were used for the observation trough and TES, while unstructured tetrahedral grids were used for other parts [25]. The numbers of grids corresponding to various structure parameters are given in Table 1.

Table 1. Numbers of grids corresponding to various structure parameters.

Structure Parameters	Length of TES (M)			Inlet Angle (θ)		
	50 mm	100 mm	150 mm	30°	45°	60°
Number of grids	295,529	274,965	257,837	244,945	257,837	239,511

Figure 3a shows the combined grids corresponding to different lengths of the TES. Figure 3b shows the grids of the inlet pipe corresponding to different inlet angles.

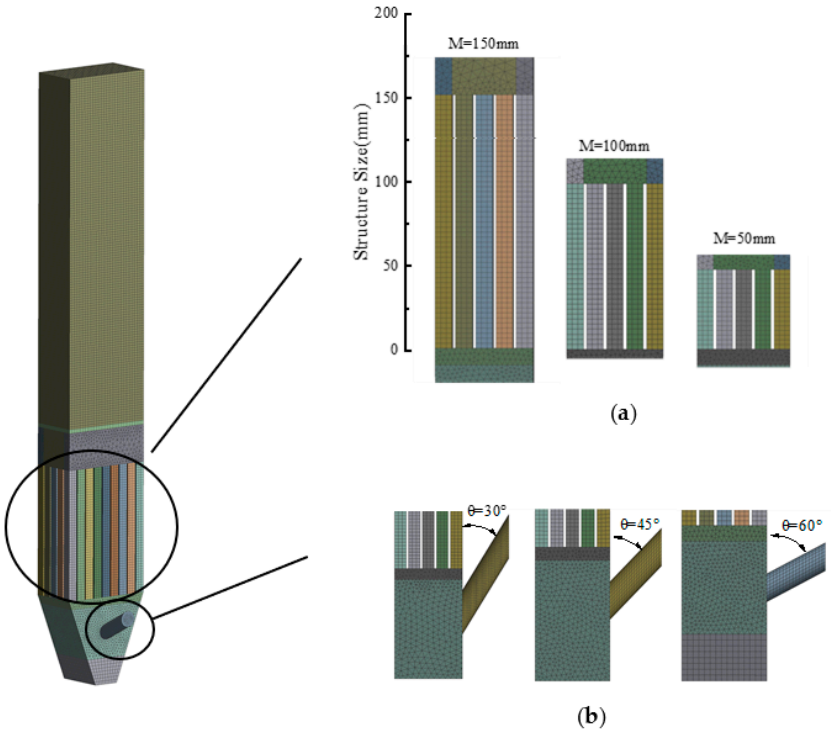

Figure 3. Grids of different structures. (**a**) Grids corresponding to different lengths of the TES. (**b**) Grids corresponding to different inlet angles.

3.2. System Settings

The standard k-epsilon turbulence model was used for numerical simulation and calculation, and the heat transfer process was not considered during the simulation. In the solution process, the SIMPLEC model was used for pressure-velocity coupling [26,27]. A second-order upwind scheme was used for the pressure gradient and momentum gradient, and a first-order upwind scheme was used for the turbulence kinetic energy and turbulent dissipation rate. The boundary conditions were set as follows: purified water was used as the medium, and the density of the fluid to be introduced into the system was set to 1000 kg/m^3; the inlet mode was set to Velocity Inlet, the outlet mode was set to Outflow; the inlet temperature was set to T = 20 °C, i.e., the viscosity of the fluid was set to $\upsilon = 1.00381 \times 10^{-3}$ m^2/s; and the inlet turbulence intensity was set to 5%. For physical walls, the standard wall functions were used, and the no-slip and no-shear conditions were set. The coordinate system settings of the geometric model are shown in Figure 1a. The origin of the coordinate system is located at the center of the bottom of the inlet nozzle, and the positive direction of the *Y*-axis is vertically upward.

4. Results and Discussion

4.1. Effect of the Length of the TES on the Flow Field

Figure 4 shows the streamline diagrams of the X = 0 m section and Z = 0 m section of the observation trough in the flow field corresponding to an inlet angle of 45° and different lengths of the TES.

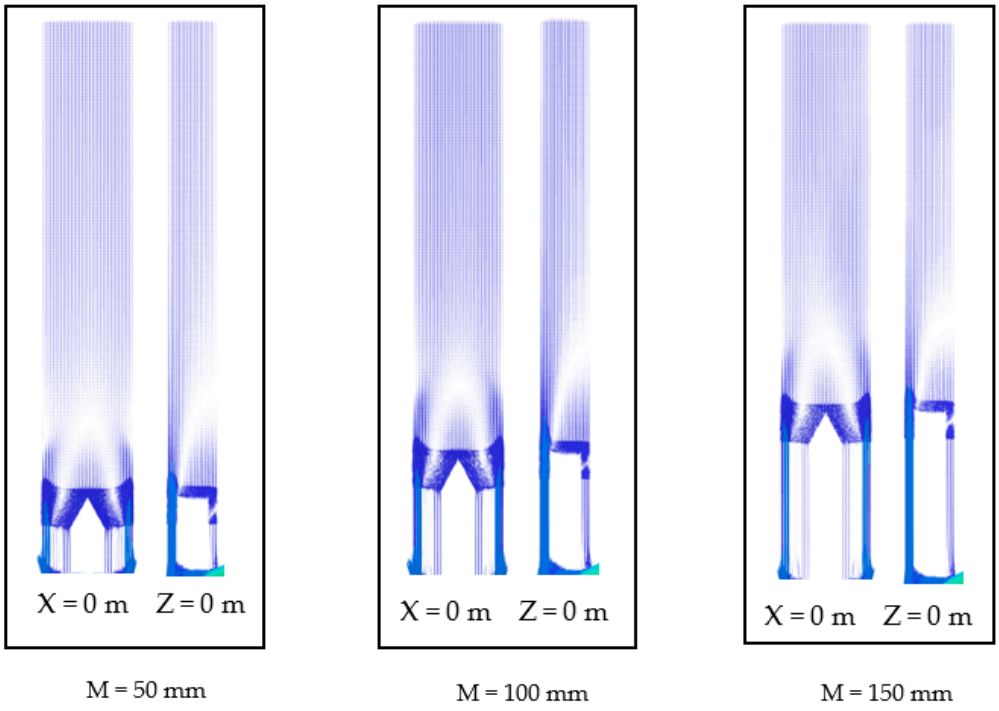

Figure 4. Streamline diagrams of different sections of the observation trough corresponding to different lengths of the TES.

It can be seen from Figure 4 that there is a large vortex zone above the TES. The fluid flow in this zone is chaotic and unstable. It can be seen from the X = 0 m section that, in this area, the liquid flows upward from both sides and flows back in the middle, showing a symmetrical vortex pattern on this section. Because the Inlet points to the negative direction of the *X*-axis, the vortex shows an asymmetric pattern on the Z = 0 m section. The closer to the Inlet, the larger the vortex zone and the higher the position.

To gain clearer understandings of the effect of the length of the TES on the internal flow field, the distribution of turbulence intensities across the Z = 0 m section and X = 0 m section was identified (as shown in Figure 5), and the distribution of the turbulence intensities of the liquid near the lower edge along the Y-axis corresponding to different lengths of the TES was measured (as shown in Figure 6). The different lengths of the TES are as follows: L_1: (0 m, 0.1 m, 0.48 m)–(0 m, 0.7 m, 0.48 m); L_2: (−0.24 m, 0.1 m, 0 m)–(−0.24 m, 0.7 m, 0 m).

Figure 6a shows the variation of turbulence intensity with the inlet velocity corresponding to L_1 across the X = 0 m section. Figure 6b shows the variation of turbulence intensity with the inlet velocity corresponding to L_2 across the Z = 0 m section. It can be found from the flow field diagram that the vortex zone is affected by the length of the TES and the inlet velocity. When the length of the TES is 50 mm and Y = 0.15 m, the flow enters the vortex zone. When the inlet velocity is 0.3 m/s, the range of the vortex zone is Y = 0.15–0.25 m. When Y > 0.25 m, the turbulence intensity starts to decrease slowly, the flow field is relatively stable, and the detection results are less affected by the internal turbulence. When the inlet velocity is 0.6 m/s, the range of the vortex zone is Y = 0.15–0.30 m. When the inlet velocity is 0.9 m/s, the range of the vortex zone is Y = 0.15–0.33 m. As the length of the TES increases, the turbulent zone moves upward. When the length of the TES reaches 150 mm, the effect of inlet velocity on the vortex zone is greatly reduced, and the vortex zone remains stable in the following range: Y = 0.25–0.35 m.

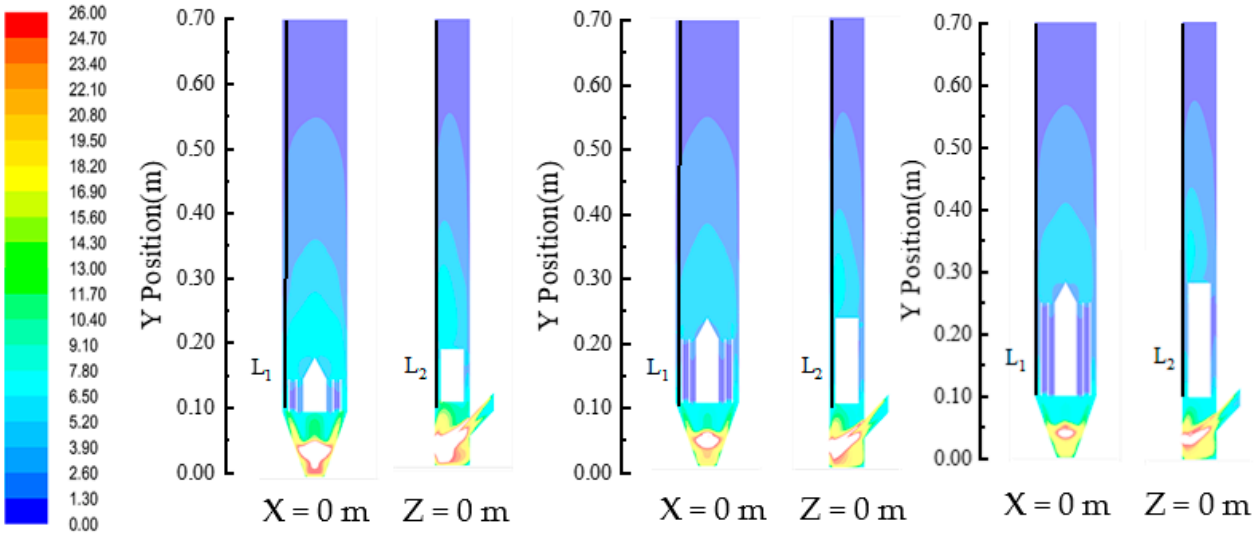

Figure 5. Distribution of turbulence intensities across different sections of the observation trough corresponding to different lengths of the TES.

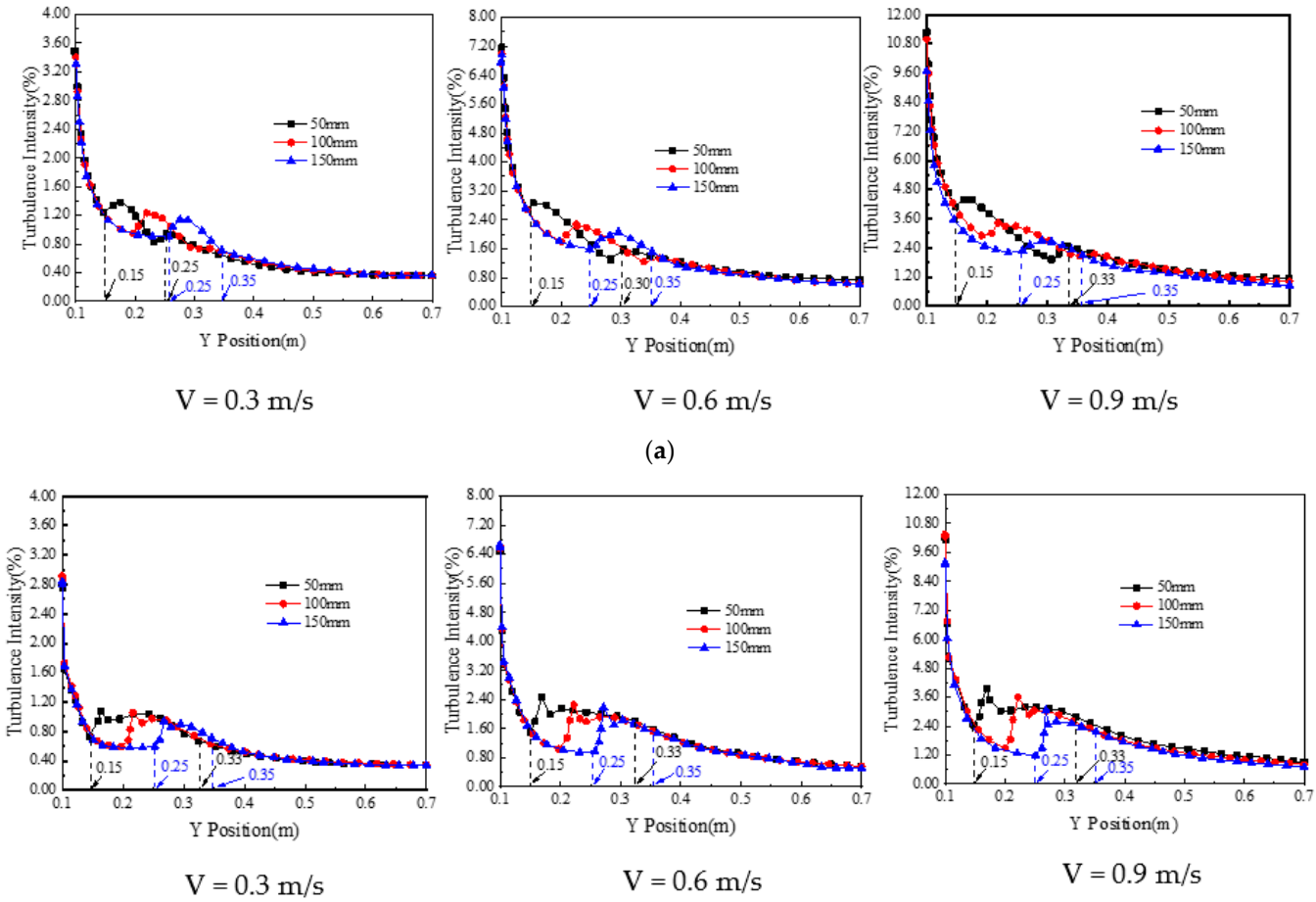

Figure 6. Charts showing the changes in turbulence intensity with the length of the TES. (**a**) Changes in turbulence intensity corresponding to L_1. (**b**) Changes in turbulence intensity corresponding to L_2.

The length of the TES also affects the distribution of turbulence intensities to a certain extent. When the flow velocity is 0.3 m/s and Y > 0.4 m, the changes in turbulence intensity in the stable zone of turbulence along the lines L_1 and L_2 corresponding to different lengths

of the TES are basically consistent. As the inlet velocity increases, the changes in turbulence intensity vary with the length of the TES. For example, when the inlet velocity is 0.9 m/s and the length of the TES is 150 mm, the turbulence intensity is slightly lower than those in the other two cases, indicating that the length of the TES can inhibit the turbulence intensity to a certain extent. In addition, the greater the inlet velocity, the more obvious such an inhibition effect will be. By comparing the turbulent intensities along L_1 and L_2, it can be known that the changes in turbulent intensity along L_1 are steadier when the inlet velocity is high. Considering the fact that a sufficiently stable zone is required for concentration detection, the length of the TES cannot be increased indefinitely. It is very reasonable to take 150 mm as the final optimal length of the TES.

4.2. Effect of the Inlet Angle on the Flow Field

Figure 7 shows the streamline diagrams of the X = 0 m section and Z = 0 m section of the observation trough in the flow field corresponding to different inlet angles. The variation of inlet angle has a great influence on the flow field distribution in the observation trough. When the inlet angle is 30°, two remarkable vortices can be observed on the Z = 0 m plane. When the inlet angle is 45°, one remarkable vortex can be observed on the Z = 0 m plane. When the inlet angle reaches 60°, the vortex zone becomes much smaller than the vortex zone corresponding to the inlet angle of 45°, and the internal flow field has basically stabilized. Moreover, the streamline direction is vertical, and a larger stable zone forms in the observation trough.

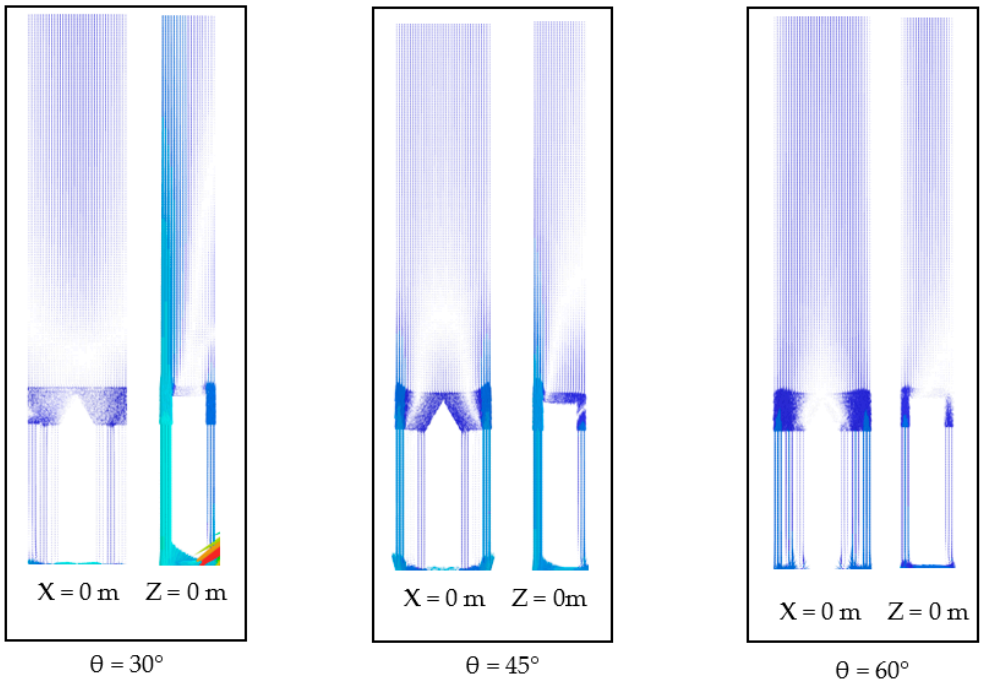

Figure 7. Streamline diagrams of different sections of the observation trough corresponding to different inlet angles.

To better understand the effect of inlet angle on the internal flow field, the distribution of turbulence intensities across the Z = 0 m section and X = 0 m section was identified (as shown in Figure 8), and the distribution of the turbulence intensities of the liquid near the measuring points along the Y-axis corresponding to different inlet angles was measured (as shown in Figure 9). The different lengths of the TES are as follows: L_1: (0 m, 0.1 m, 0.48 m)–(0 m, 0.7 m, 0.48 m); L_2: (−0.24 m, 0.1 m, 0 m)–(−0.24 m, 0.7 m, 0 m).

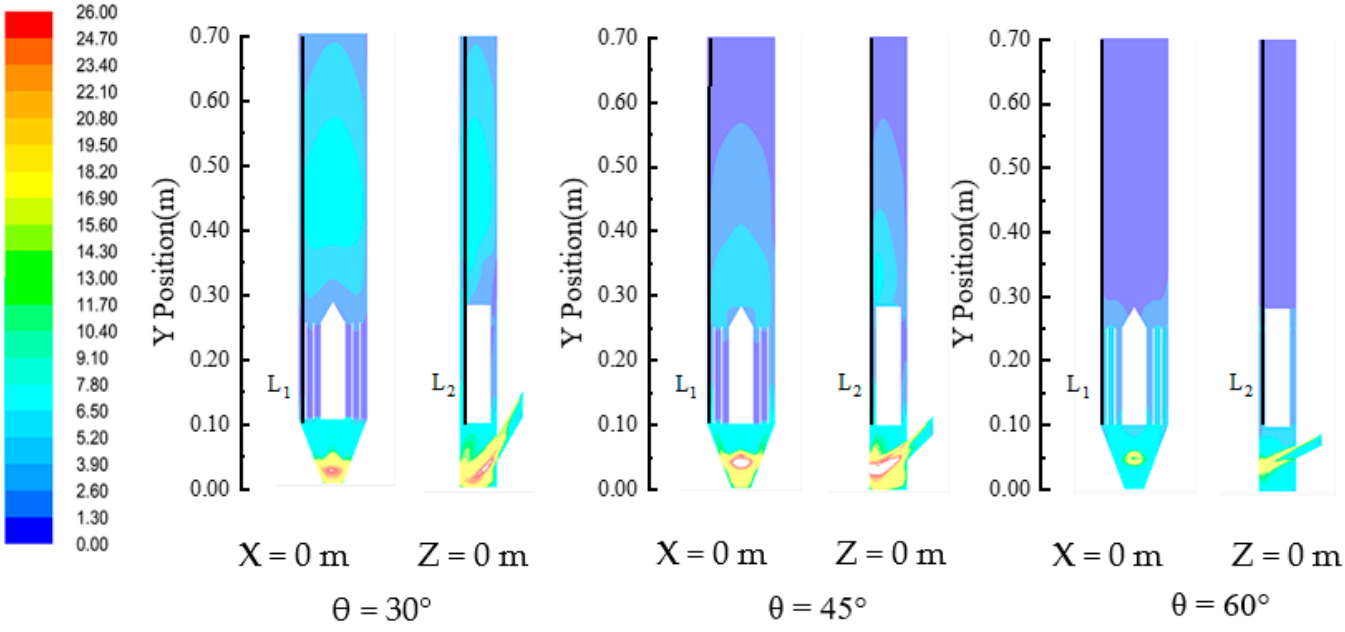

Figure 8. Distribution of turbulence intensities across different sections of the observation trough corresponding to different inlet angles.

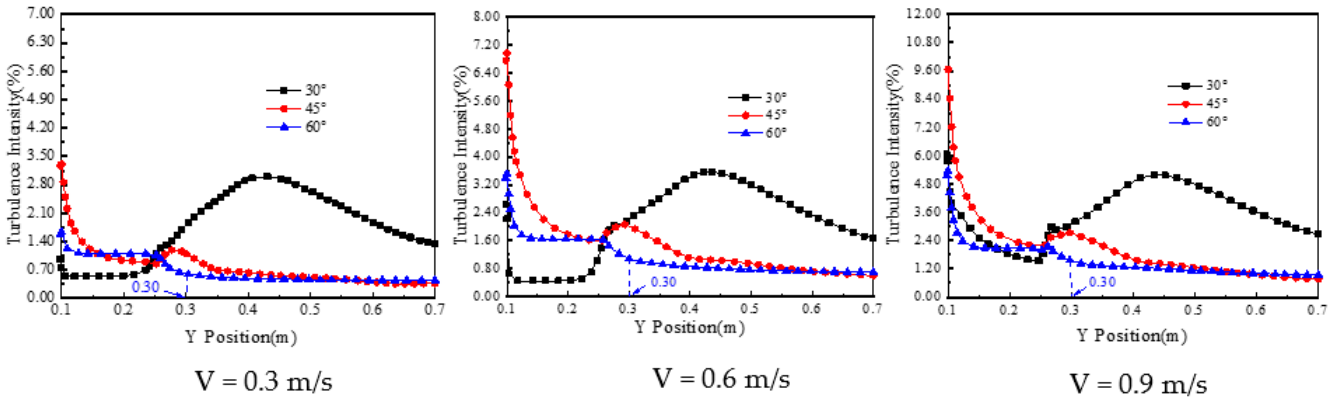

(**a**)

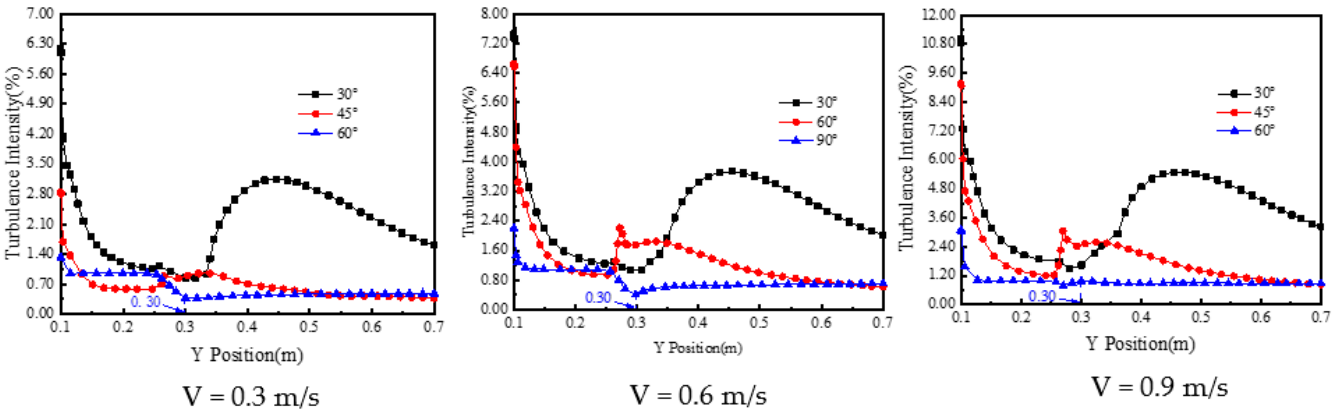

(**b**)

Figure 9. Graph showing the changes in turbulence intensity along the Y-axis with the inlet angle. (**a**) Changes in turbulence intensity along the Y-axis corresponding to L_1. (**b**) Changes in turbulence intensity along the Y-axis corresponding to L_2.

Figure 9a shows the distribution of turbulence intensities along L_1 on the X = 0 m section. Figure 9b shows the distribution of turbulence intensities along L_2 on the Z = 0 m section. From the charts showing the distribution of turbulence intensities along L_1, it can be seen that when the inlet angle is 30°, two remarkable peaks of turbulence intensity appear. By analyzing the flow field diagram, it can be known that the positions of the two peaks are the centers of vortices in the flow field. The reason for the appearance of two peaks is that two vortices have been generated in the flow field. As the inlet velocity increases, the peak of turbulence intensity gradually rises and moves toward the positive direction of the *Y*-axis, indicating that the vortex zone gradually rises with the increase in inlet velocity. This trend is consistent with the conclusion drawn when the variable is the length of the TES. As the inlet angle increases, the peak of turbulence intensity declines gradually. The results of observation for the inlet angle of 60° show that the turbulence intensity is stable when Y > 0.3 m. When the inlet velocity is lower than 0.9 m/s, a stable zone of turbulence can always be formed, which can effectively reduce the errors caused by the flowing liquid during measurement.

4.3. Study of the Measuring Accuracy of the Experimental Device

Experiments was conducted using clean water as the medium, and the values of differential pressure (ΔP) at different inlet velocities were obtained through these experiments. The theoretical differential pressure was theoretically calculated. For these experiments, the maximum allowable error is 1%. The experimental results are shown in Figure 10.

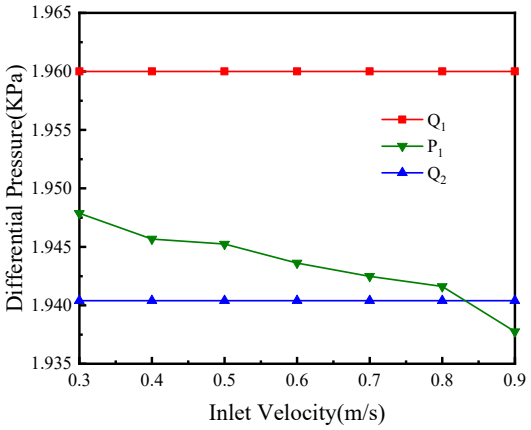

Figure 10. Chart showing the changes in the measured differential pressure (in clean water) with the inlet velocity.

In Figure 10, Q_1 is the theoretical differential pressure, P_1 is the detected differential pressure, and $Q_2 = (1 - 1\%)Q_1$, which denotes the lowest value of differential pressure when the allowable detection error is 1%.

Given that ΔH = 20 cm, the calculated values of Q_1 and Q_2 are as follows: Q_1 = 1.960 KPa, Q_2 = 1.940 KPa. It can be known from Figure 10 that when clean water is used as the medium, the detected differential pressure is always lower than the theoretical differential pressure and tends to deviate from the theoretical differential pressure as the inlet velocity increases. When the inlet velocity V $\leq$ 0.8 m/s, the detection error is not more 1% and meets the requirements for detection accuracy.

4.4. Study of Detection Accuracy at Different Densities

To further investigate the effect of inlet velocity on the stability of detection sensors, we analyzed the errors in the experimental results corresponding to inlet velocities ranging from 0.3 m/s to 0.9 m/s. The equation used for this error analysis is as follows:

$$\eta_{ij} = \left| \frac{p_{ij} - p_{0j}}{p_{0j}} \right| \times 100\% (i = 1,2,3,4,5,6,7; j = 1,2,3) \quad (3)$$

where η_{ij} is the error between the detected differential pressure and the theoretical differential pressure, p_{ij} is the detected differential pressure, and p_{0j} is the theoretical differential pressure.

Figure 11 shows the changes in detection error with inlet velocity. Table 2 shows the calculated theoretical differential pressures corresponding to liquids of different densities. In all experimental results, the detection errors for the low-density liquid are greater than those for the high-density liquid, but the detection errors are generally within a reasonable range of 1%. When the inlet velocity reaches 0.9 m/s, the detection error for the low-density liquid becomes greater, and the detection stability is greatly reduced. Therefore, it can be determined that the optimal operating conditions of the concentration detection system will be achieved when V $\leq$ 0.8 m/s. The influence of liquid density on the flow regime in the model and related parameters needs to be controlled by adjusting the inlet velocity based on the actual operations conditions to improve the overall performance of the system in concentration detection.

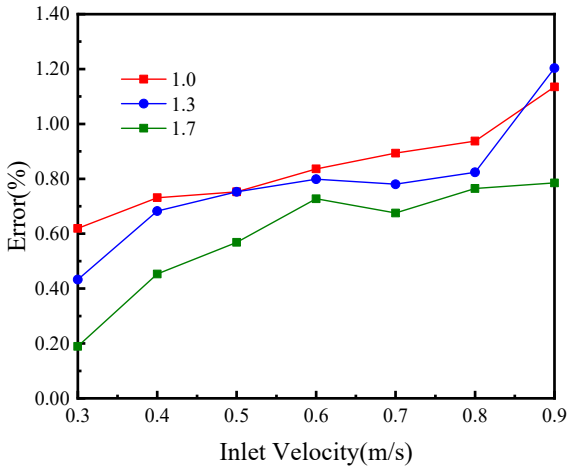

Figure 11. Chart showing the changes in detection error with inlet velocity corresponding to different liquid densities.

Table 2. Theoretical differential pressures corresponding to liquids of different densities (ΔH = 20 cm).

Density (g/mL)	1.0	1.3	1.7
Theoretical differential pressure (KPa)	1.960	2.548	3.332

5. Conclusions

The numerical simulation results of TES with different lengths show that the eddy current region is affected by the TES length and inlet velocity. The longer the TES, the higher the stability of turbulence intensity in the observation trough. When the inlet velocity increases to 0.9 m/s, the distribution of turbulence intensity changes significantly with the length of TES. The longer the TES, the lower the turbulence intensity.

The simulation results of different inlet angles show that the peak turbulence intensity decreases with the increase of the inlet angle. When the inlet angle is 60°, the turbulence intensity on the upper part of the concentration detection device is stable, and a stable turbulence zone is formed, which can effectively reduce the detection error and improve the detection accuracy.

The experimental results show that when the TES length is 150 mm and the inlet angle is 60°, the change of detection error of low-density liquid is greater than that of high-density liquid, but the detection error is within a reasonable range. When V $\leq$ 0.8 m/s, the test result is reasonable and effective. Adjust the inlet velocity according to the actual operating conditions to improve the concentration detection performance of the system.

Author Contributions: Conceptualization, Z.L. and C.W.; methodology, Z.L. and C.W.; software, H.L. and J.C.; validation, Z.L. and J.C.; formal analysis, Z.L., C.W. and Q.Z.; investigation, Z.L., H.L. and C.W.; resources, H.L. and C.W.; data curation, Z.L. and Q.Z.; writing—original draft preparation, Z.L.; writing—review and editing, C.W.; visualization, J.C.; supervision, H.L.; project administration, H.L.; funding acquisition, H.L. All authors have read and agreed to the published version of the manuscript.

Funding: This work was financially supported by the research fund of the Provincial University Natural Science Research of Anhui Province (Grant No. 1908085QE189), the Postdoctoral Research Project of Anhui (Grant No. 2019B356), and the Scientific Research Foundation for High-level Talents of Anhui University of Science and Technology (Grant No. 11885).

Data Availability Statement: The data that support the findings of this study are available from the corresponding author (H.L.), upon reasonable request.

Conflicts of Interest: All authors declare no relevant relationships.

References

1. Wang, Y.; Wang, Y.; Xiao, W.; Wei, Y.; Li, S. Effect of Cu^{2+} on the activation to muscovite using electrochemical pretreatment. *Minerals* **2020**, *10*, 206. [CrossRef]
2. Mehmood, M.A.; Ibrahim, M.A.; Ullah, A.; Inayat, M.H. CFD study of pressure loss characteristics of multi-holed orifice plates using central composite design. *Flow. Meas. Instrum.* **2019**, *70*, 101654. [CrossRef]
3. Twu, R.-C.; Chen, J.-Y. A compact displacement sensor for non-intrusive concentration measurements of flowing liquid. *Sens. Actuators A Phys.* **2017**, *267*, 424–430. [CrossRef]
4. Rawat, A.; Singh, S.N.; Seshadri, V. CFD analysis of the performance of elbow-meter with high concentration coal ash slurries. *Flow. Meas. Instrum.* **2020**, *72*, 101724. [CrossRef]
5. Bilge, G.; Sezer, B.; Boyaci, I.H.; Eseller, K.E.; Berberoglu, H. Performance evaluation of laser induced breakdown spectroscopy in the measurement of liquid and solid samples. *Spectrochim. Acta Part B At. Spectrosc.* **2018**, *145*, 115–121. [CrossRef]
6. Zhu, Q.; Yang, X.; Wang, G.; Yan, Y.; Schlegel, J.P.; Liu, Y.; Hilger, R.T.; Buchanan, J.R.; Ishii, M. Two-sensor droplet-capable conductivity probe for measurement in liquid dispersed flows. *Ann. Nucl. Energy* **2021**, *150*, 107827. [CrossRef]
7. He, D.; Bai, B.; Xu, Y.; Li, X. A new model for the v-cone meter in low pressure wet gas metering. *Meas. Sci. Technol.* **2012**, *23*, 125305. [CrossRef]
8. David, F.; Ismail, A.; Robert, M.B. In-situ investigation on real-time suspended sediment measurement techniques: Turbidimetry, acoustic attenuation, laser diffraction (lisst) and vibrating tube densimetry. *Int. J. Sediment Res.* **2018**, *33*, 3–17.
9. Passos, M.L.C.; Saraiva, M.L.M. Detection in uv-visible spectrophotometry: Detectors, detection systems, and detection strategies. *Measurement* **2019**, *135*, 896–904. [CrossRef]
10. Bayram, A.; Yalcin, E.; Demic, S.; Gunduz, O.; Solmaz, M.E. Development and application of a low-cost smartphone-based turbidimeter using scattered light. *Appl. Opt.* **2018**, *57*, 5935–5940. [CrossRef]
11. Mohd, T.M.K.; Sallehuddin, I.; Mohd, A.M.Y.; Mahdi, F. A review on the design and development of turbidimeter. *Sens. Rev.* **2015**, *35*, 98–105. [CrossRef]
12. Sampedro, Ó.; Salgueiro, J.R. Turbidimeter and RGB sensor for remote measurements in an aquatic medium. *Measurement* **2015**, *68*, 128–134. [CrossRef]
13. Ebie, K.; Yamaguchi, D.; Hoshikawa, H.; Shirozu, T. New measurement principle and basic performance of high-sensitivity turbidimeter with two optical systems in series. *Water Res.* **2006**, *40*, 683–691. [CrossRef]
14. Rai, A.K.; Kumar, A. Continuous measurement of suspended sediment concentration: Technological advancement and future outlook. *Measurement* **2015**, *76*, 209–227. [CrossRef]
15. Thorne, P.D.; Hurther, D. An overview on the use of backscattered sound for measuring suspended particle size and concentration profiles in non-cohesive inorganic sediment transport studies. *Cont. Shelf. Res.* **2014**, *73*, 97–118. [CrossRef]
16. Zheng, H.; Su, Y.; Zheng, L.; Ke, H. Numerical simulation of CO_2 and dye separation for supercritical fluid in separator. *Sep. Purif. Technol.* **2020**, *236*, 116246. [CrossRef]
17. Peng, S.; Liao, W.; Tan, H. Performance optimization of ultrasonic flow meter based on computational fluid dynamics. *Adv. Mech. Eng.* **2018**, *10*, 1687814018793264. [CrossRef]
18. Lee, H.H.; Jang, S.B.; Shin, G.W.; Hong, S.T.; Lee, D.J.; Chun, M.G. An ultrasonic multi-beam concentration meter with a neuro-fuzzy algorithm for water treatment plants. *Sensors* **2015**, *15*, 26961–26977. [CrossRef]
19. Wrobel, B.M.; Time, R.W. Ultrasonic measurement and characterization of a low concentration system of solid particles in liquid, in high shear flow. *Appl. Acoust.* **2012**, *73*, 117–131. [CrossRef]
20. Song, Y.; Zhao, W.; Huang, Y.; Li, D. Underwater bubble detection and counting by a dynamic changing solid-liquid interfacial process. *Sens. Actuators B Chem.* **2021**, *329*, 129083. [CrossRef]
21. Jens, R.; Michael, M. Concentration measurement in bubbly liquids—A matter of times. *Phys. Procedia* **2015**, *70*, 147–150.
22. Kim, J.-Y.; Lee, J.-H.; Bae, S.-E.; Paek, S.; Kim, S.H.; Kim, T.-J.; Park, T.-H. Automated high-temperature liquid level measurement system using a dynamic tube pressure technique. *J. Ind. Eng. Chem.* **2017**, *49*, 30–35. [CrossRef]

23. Zhang, F.; Dong, F.; Tan, C. High gvf and low pressure gas–liquid two-phase flow measurement based on dual-cone flowmeter. *Flow Meas. Instrum.* **2010**, *21*, 410–417. [CrossRef]
24. Pankaj, K.R.; Santosh, K.S.; Koustuv, D. Turbulence characteristics of oscillating flow through passive grid. *Ocean Eng.* **2021**, *224*, 108727.
25. Wang, C.; Wang, C.; Xie, J.; Khan, M.S. Influence mechanism of gas–containing characteristics of annulus submerged jets on sealing degree of mixing zone. *Processes* **2022**, *10*, 593. [CrossRef]
26. Zolfagharnasab, M.H.; Salimi, M.; Aghanajafi, C. Application of non-pressure-based coupled procedures for the solution of heat and mass transfer for the incompressible fluid flow phenomenon. *Int. J. Heat Mass Transf.* **2021**, *181*, 121851. [CrossRef]
27. Wang, C.; Wang, C.; Yu, A.; Zheng, M.; Khan, M.S. Effect of closure characteristics of annular jet mixed zone on inspiratory performance and bubble system. *Processes* **2021**, *9*, 1392. [CrossRef]